Hindawi
Advances in Materials Science and Engineering
Volume 2021, Article ID 7752352, 11 pages
https://doi.org/10.1155/2021/7752352

Research Article

The Influences of Sand Content and Particle Size on the Desiccation Cracks of Compacted Expansive Soil

Dongdong Li [1,2] **and Shaowei Zhang** [1,3]

[1]*School of Civil Engineering and Architecture, Xi'an University of Technology, Xi'an, Shanxi 710048, China*
[2]*School of Civil Engineering, Xuchang University, Xuchang, Henan 461000, China*
[3]*School of Civil & Architecture Engineering, Xi'an Technological University, Xi'an, Shanxi 710021, China*

Correspondence should be addressed to Dongdong Li; ldd@xcu.edu.cn and Shaowei Zhang; zhangshaowei@xatu.edu.cn

Received 5 July 2021; Accepted 13 September 2021; Published 24 September 2021

Academic Editor: Hao Yi

The desiccation cracks in expansive soil, which are a common natural phenomenon, have a significant negative impact on the engineering properties of the soil and are the direct cause of many engineering problems and geological disasters. This study aims to investigate the influences of sand content and particle size on desiccation cracks of the compacted expansive soil. First, samples of compacted expansive soil with five sand contents and four sand size groups were prepared. Then, a series of drying tests were performed. The dynamic variation of geometric parameters of the surface crack network during evaporation was quantitatively analyzed by using digital image processing technology and fractal theory. The results demonstrated that the increase of the surface-cracking areas in the early and later stages was manifested by the increase of the crack length and crack width, respectively. In the same size of sand particle group (0.15, 0.3 mm), as the sand content (dry weight ratio of soil sample) increased from 0% to 40%, the surface-cracking ratio (the ratio of the crack area to the total surface area of the soil sample) showed a decreasing trend (13.20%, 11.42%, 10.50%, 8.98%, and 7.71%, respectively). When the sand content (40%) was the same, as the sand size groups increased from [0.15 mm, 0.3 mm) to [1.18 mm, 2.36 mm), the surface-cracking ratio also presented a decreasing trend (7.71%, 7.69%, 4.35%, and 3.73%, respectively). The changing law of the fractal dimension of cracks was the same as that of the surface crack ratio. During the drying process, the deformation of the sample was characterized by centripetal shrinkage or cracking, which were mainly affected by the boundary conditions of the sample. This research's results verify the effectiveness of sand to improve the dry-shrinkage characteristics of expansive soil, providing a reference for the improvement of roadbeds and the treatment of soil slopes in expansive soil areas.

1. Introduction

Expansive soil is rich in minerals with strong hydrophilicity such as montmorillonite and illite. It is a kind of clay with significant swelling, shrinkage, and cracking properties, widely distributed in the world [1]. The physical and mechanical properties of expansive soil are sensitive to climate change. This is extremely harmful to engineering constructions such as roadbeds and slopes [2, 3]. In recent years, due to global climate change, extreme arid climates have occurred more frequently, and the damage caused by shrinkage and cracking of expansive soils has become more prominent.

Desiccation cracks caused by the evaporation of water in soil are a common natural phenomenon. The desiccation cracks in soil have adverse effects on several fields such as agriculture, geology, and geotechnical engineering. The cracks in farmland soil will aggravate drought, increase soil strength, and adversely affect plant root growth, resulting in the reduction of crop yields [4]. From another perspective, the cracks cause preferential flow during irrigation or rainfall, leading to a decrease in the efficiency of water and fertilizer utilization, but an increase in the risk of groundwater pollution [5, 6]. The cracking network on the soil slope can destroy the integrity of the soil and provide convenient conditions for rainwater infiltration, contributing to

significantly weakening the shear strength of the soil and inducing landslides [7–9]. Desiccation cracks in the foundation or roadbed can reduce the bearing capacity of the soil, inducing some problems such as uneven settlement and pavement cracking [10].

A large number of studies have been conducted on the influencing factors of soil desiccation cracks and the quantitative analysis of crack morphology [11, 12]. Costa et al. performed desiccation experiments on three materials: clay, potato starch, and milled quartz sand. The results suggested that the development process and final cracking morphology of different materials are quite different [13]. Tang et al. explored the effects of temperature, soil layer thickness, dry-wet cycle, and soil type on the geometric parameters of desiccation cracks of the initial clay slurry samples by using image processing technology [14]. Abou Najm et al. researched the influence of the solute contents in the pore water on the shrinkage deformation of the soil. The results demonstrated that the evaporation rate of water, shrinkage rate, and drying stress all decreased with the increasing concentration of NaCl in the pore water [15]. Yesiller et al. investigated the desiccation cracking of compacted liner soils. The results indicated that the surface-cracking ratio increased with the increase of the fine-grained soil content and the initial water content, as well as the effect of the dry-wet cycles [16].

Expansive soil in engineering should be improved to handle the hazards caused by its unstable engineering properties. At present, the approaches to improve expansive soil mainly include physical and chemical methods, biological, and solid waste improvement technologies [17, 18]. The most commonly used method is a chemical improvement, such as mixing lime, cement, and fly ash. AlZubaidi et al. pointed out that the swelling potential, linear shrinkage rate, and clay mineral content of expansive soil decreased with the increase in cement percentage [19]. Stoltz et al. explored the effects of wetting and drying paths on the expansion and contraction of lime-treated expansive soil. The results revealed that lime-treated compacted expansive soil could effectively prevent volume expansion during initial wetting. However, the inhibition effect on shrinkage during drying was limited [20]. Kalkan prepared compacted soil samples under optimal water content conditions using the mixture of silica fume and clay and conducted dry-wet cycle and expansion tests. The results reflected that silica fume could reduce the progressive deformation of improved expansive clay under the action of dry-wet cycles [21]. Ikizler et al. discovered that mixing sand with bentonite or placing sand on top of bentonite could reduce the swelling force of bentonite. Specifically, the swelling force of the sand-bentonite mixture decreased as the sand content increased [22].

In the past, a considerable number of studies have been conducted on the mechanical properties of the improved expansive soils. Nevertheless, there is little research on the desiccation shrinkage characteristics of improved expansive soil. Compared with fine materials such as cement and fly ash, sand has a certain hardness and larger particle size. Thus, the sands are easier to mix with soil. Moreover, the construction is simple without environmental pollution. Therefore, the sands were used as an improved material in this study, and a series of drying tests were performed to investigate the influence of sand content and particle size on desiccation cracks of compacted expansive soil samples. Image processing technology and fractal theory were adopted to analyze the characteristics of the surface desiccation cracks of the expansive soil improved by sands.

2. Materials and Methods

2.1. Materials. Soil samples for the test were taken at a depth of 0.8–1.5 m below the land surface from a landslide-monitoring site in Mian County, Shaanxi Province, China. The location of the collected soil is illustrated in Figure 1. The undisturbed soil samples were wrapped with plastic film and sealed with adhesive tape to prevent water loss. The water content and dry density of undisturbed soil samples were determined by the ring knife method in the laboratory. The soils were air-dried, crushed, and passed through a 2 mm sieve. The physical properties of the soil samples, such as specific gravity limit, water content, and free swelling rate, etc., were tested according to the Chinese standard for geotechnical testing method (GB/T 50123–2019). Among them, the free swelling rate, defined as the ratio of the increased volume after stable deposition in water to the initial volume of the oven-dried and crushed fine-grained soil, was measured by a glass-measuring cylinder with the volume of 50 mL and the division value of 1 mL. The physical and mechanical properties of soil are presented in Table 1. It can be seen that the test soil is composed of fine-grained soil with a liquid limit greater than 50%, according to the standard (GB/T 50145–2007, GB 50112–2013); the test soil is high liquid limit clay (CH) with weak expansibility. The particle size distribution of the sample was measured with a laser particle size analyzer (Bettersize 2000; measurement range: 0.02–2000 μm), as exhibited in Figure 2. The particle size analyses of the testing soil indicated that its clay and silt contents were 44.8% and 55.25%, respectively, with no sand particles inside. The mineral composition and its approximate percentage of the soil sample were determined by an x-ray diffractometer (Bruker D8 advance), as illustrated in Table 1. The results showed that the main components of clay minerals were 32.89% illite, 9.23% kaolinite, and 6.61% smectite. The standard sand (China ISO Sand Co., Ltd.) was used for the test, and its grading curve is displayed in Figure 2.

2.2. Experimental Scheme and Process. The test process is presented in Figure 3. The soil and standard sand used to prepare the samples were dried at 105°C to the constant weight. The soil was crushed and passed through a 2 mm sieve. Then, different particle size groups of standard sands were separated through a sieving test, as shown in Figure 3(a). Besides, the samples were prepared with higher initial water content and lower dry density to observe the obvious development of desiccation cracks. Sand with a specific particle size range and content was added to the soil sample and mixed evenly. Then, distilled water was sprayed

Figure 1: Studied area and sampling location.

Table 1: Basic physical properties and mineral composition of clayey soil samples.

Soil properties	Value	Mineral composition	(%)
Undisturbed soil density (g/cm^3)	1.76	Illite	32.89
Undisturbed soil water content (%)	18.5	Kaolinite	9.23
Specific gravity	2.72	Chlorite	7.09
Atterberg limits		Smectite	6.61
Liquid limit (%)	52	Quartz	29.63
Plastic limit (%)	25	Else	14.55
Plasticity index	26.5		
Particle size analysis			
Sand (%)	0		
Silt (%)	55.2		
Clay (%)	44.8		
Free swelling ratio (%)	65.5		

to prepare a sand-soil mixture with an initial water content of 25% and then sealed for 48 hours to ensure that the water was fully diffused. Using the static pressure method, the sample with a dry density of 1.35 g/cm^3 was prepared in a glass evaporating dish with a diameter of 100 mm and a height of 19.5 mm. The surface of the soil samples was smoothed with a stainless-steel knife. The prepared samples were put into a ziplock bag for 24 hours to make the water in the sample evenly distributed.

The experimental design is illustrated in Table 2, with a total of eight groups of experiments, three parallel samples in each group. The prepared samples are presented in Figure 3(b), in which S1–S5 and S5–S8 were used to investigate the influence of sand content and particle size on the desiccation cracks of expensive soil, respectively.

The oven-drying method was adopted to promote the evaporation of water and shorten the test time with the evaporation temperature at 50°C (Figure 3)(c). During the drying process, the soil samples were taken out, weighed, and photographed at 0.5-hour intervals. The digital camera (Nikon D850 with a resolution of 45.7 megapixels) was connected to the computer via Wi-Fi, and the acquired images could be automatically stored in the computer. In the process of image acquisition, the distance between the camera and the sample was fixed, and all external light sources were blocked. Only led lighting was applied to the consistent photographing environment. The test ended when the sample mass change was less than 0.1 g.

2.3. Image Processing. The digital image processing technology was used to quantitatively analyze the evolution of desiccation cracks during evaporation [23, 24]. The image processing process is exhibited in Figure 4. In the first step, the original image was extracted along the inner edge of the glass container for analysis, with the irrelevant image information removed (Figure 4(a)). In the second step, the weighted average method was used to obtain the gray image, which converted RGB values to grayscale values by using equation (1) to form a weighted sum of the R, G, and B components (Figure 4(b)).

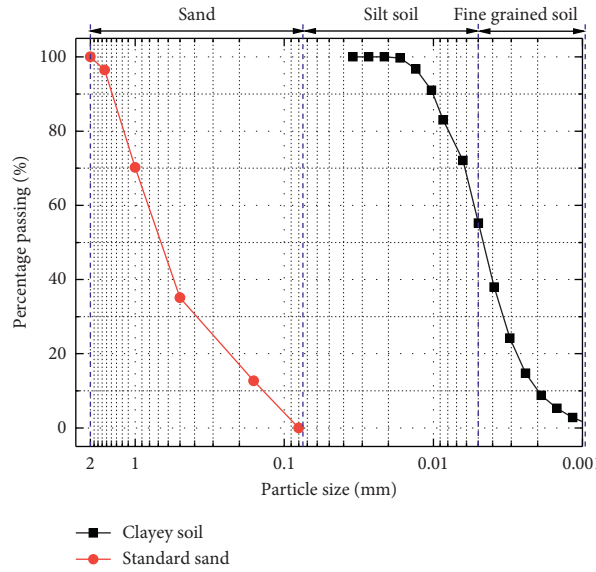

Figure 2: Particle size distributions of clayey soil and standard sand.

$$\text{Gray} = i * R + j * G + k * B, \tag{1}$$

where R, G, and B represent the red, green, and blue color components of a pixel, respectively, and i, j, and k are the weight coefficients.

In the third step, Otsu's method was adopted to calculate the optimal threshold and convert the gray image into a binary image [25], in which the black and white areas represented cracks and soil blocks, respectively (Figure 4(c)). The optimal threshold (T) could be obtained by the following equations:

$$w_1 = \frac{n_1}{N}, \tag{2}$$

$$w_2 = \frac{n_2}{N} = 1 - w_1 = 1 - \frac{n_1}{N}, \tag{3}$$

$$u_1 = \frac{\sum_{i=0}^{T} i * P_i}{\sum_{i=0}^{T} P_i}, \tag{4}$$

$$u_2 = \frac{\sum_{i=T+1}^{255} i * P_i}{\sum_{i=T+1}^{255} P_i}, \tag{5}$$

$$u = u_1 * w_1 + u_2 * w_2, \tag{6}$$

$$g = w_1 * w_2 * (u_1 - u_2)^2. \tag{7}$$

The optimal threshold T divides the image into two groups: target and background, where N is the total number of image pixels; i and P_i are the gray value and corresponding numbers of the pixel; n_1 and n_2 are the numbers of pixels whose grayscale value less than T or greater than T; w_1 and w_2 are ratios of the number of pixels in target and background group to the image's total pixels, respectively; u_1 and u_2 are the average grayscale value of the target and background group; u is the average grayscale value of the entire image; and g is the variance between the target and background group. Otsu's threshold is used to determine the gray value T that could maximize the variance g.

In the fourth step, the morphological method, such as opening and closing operations on the morphology, was used to remove noise, fill holes, and bridge cracks in the binary image (Figure 4(d)). The main algorithms used in image morphology processing mainly include dilation, erosion, opening, and closing operation, which are defined by the following equations, respectively.

$$A \oplus B = \left\{ z \middle| (\widehat{B})_z \cap A \neq \varnothing \right\}, \tag{8}$$

$$A \odot B = \left\{ z \middle| (B)_z \subseteq A \right\}, \tag{9}$$

$$A \circ B = (A \odot B) \oplus B, \tag{10}$$

$$A \bullet B = (A \oplus B) \odot B, \tag{11}$$

where A is a set of foreground pixels, B is a structuring element, and $\widehat{B}$ is the set of points in B whose (x, y) coordinates have been replaced by $(-x,-y)$. The opening can smooth the target outline and break small connections, while the closing can bridge fractures and fill holes. The character of the cracking network in the binary image could be improved by reusing opening and closing operations several times. Finally, the skeleton of the cracking image with the width of 1 pixel after denoising was extracted (Figure 4(e)).

The analysis parameters of the surface-cracking network were evaluated by the crack ratio, length, average width, and fractal dimension. The crack ratio δ_c is defined as the ratio of the crack area S_c to the surface total area S_T of the sample and can be calculated from the ratio of the number of black pixels n_b in the denoised binary image to the total number of pixels n_T in the image, according to equation (12). Based on the cracking skeleton image, the number of black pixels on the skeleton line was calculated to obtain the approximate crack

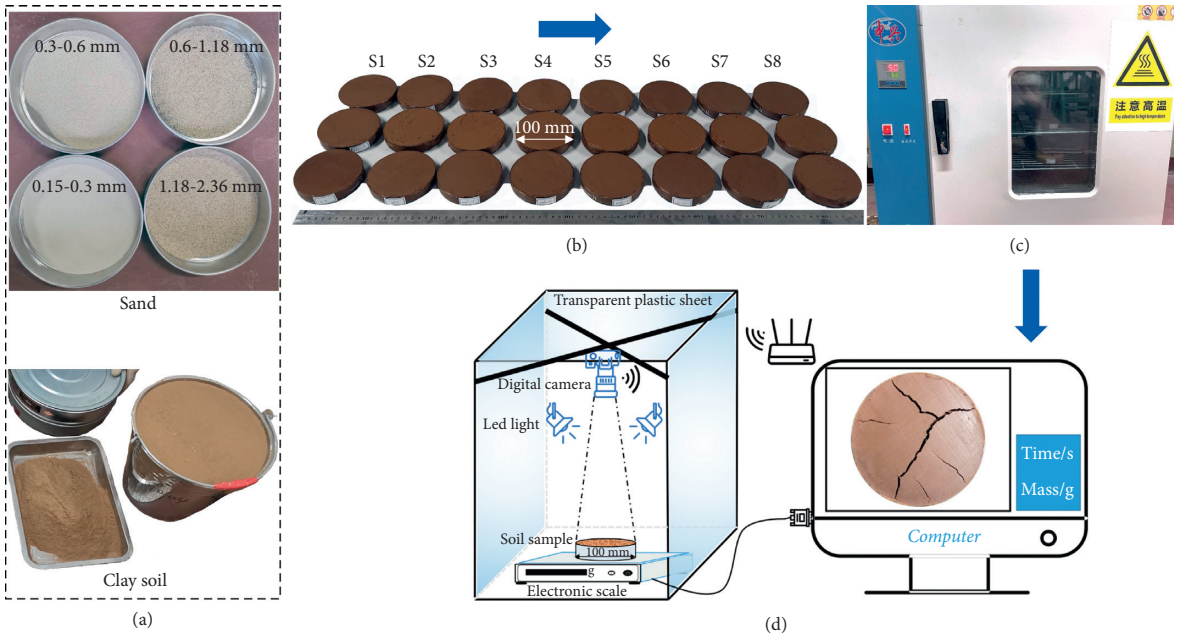

FIGURE 3: Sample preparation and experimental process. (a) Soil and standard sand after sieving. (b) Compacted soil samples. (c) Drying of soil samples. (d) Weighing and photographing device.

length L_c. The average width d of the crack is defined as the ratio of the crack area S_c to the crack length L_c, calculated by equation (13). The fractal dimension (D) of the crack could reflect the irregularity of the crack network and may be calculated by the box-counting method [26]. The crack area was covered by grids with a side length of ε, and the number of the total grids $N(\varepsilon)$ changes with the grid length ε. The relationship between $N(\varepsilon)$ and ε in the double logarithm coordinate system is expressed by the linear fitting equation (14), where D represents the value of the fractal dimension.

$$\delta_c = \frac{S_c}{S_T} = \frac{n_b}{n_T}, \tag{12}$$

$$d = \frac{S_c}{L_c}, \tag{13}$$

$$\lg N(\varepsilon) = B - D\lg(\varepsilon). \tag{14}$$

3. Results

3.1. Water Evaporation Process. Figure 5 illustrates the curve of the water content in the compacted soil sample during the drying process under the conditions of different sand contents and particle size groups. In Figure 5(a), the changing trend of the drying curves of samples with the same particle size group [0.15–0.3 mm) was the same under different sand contents. The decreasing trend of water content was approximately linear with the evaporation time in the initial stage of drying, which was the constant evaporation stage. As the evaporation continued, the drying curve gradually showed a concave shape, entering the failing evaporation stage. Finally, the drying curve gradually approached the horizontal line, and the water content no longer changed, reaching the residual water content state. As the sand content increased from 0 to 40%, the absolute value of the slope of the drying curve increased, suggesting that the water evaporation rate increased correspondingly. The time t1-t5 for the drying curve to enter the failing stage decreased in turn (18.4 h, 12.5 h, 11.4 h, 10.5 h, and 9.9 h, respectively). At the end of the test, the residual water content of the sample was 5.66%, 5.16%, 4.91%, 3.3%, and 3.17%, respectively, decreasing gradually with the increase in sand content.

Figure 5(b) presents the variation of the drying curve of sand with different particle size groups at the same sand content (40%). It also could be divided into three stages: a constant evaporation stage, a failing evaporation stage, and a residual water content stage. With the increase in sand particle size groups, the absolute value of the slope of the drying curve decreased successively, and the time t5-t8 to enter the failing evaporation stage increased in turn (9.9 h, 11.01 h, 11.9 h, and 13 h, respectively). The residual water contents of the samples were between 3.17% and 4.13%, with no significant difference.

3.2. Quantitative Analysis of Surface Cracks. The surface crack ratio could reflect the cracking degree of the sample as a whole. Figure 6(a) exhibits the variation curve of crack ratio over water content during the process of evaporation under different sand contents with the same particle size group sand [0.15–0.3 mm). The cracking water contents (the water content when cracks appeared) were all near the initial water content of the samples. After the initiation of the cracks, the surface crack ratio of the samples with different sand contents rapidly increased and then tended to be stable during the drying process. Subsequently, the crack area no

Table 2: The information of different sets of compacted samples.

Sets	Water content (%)	Dry density (g/cm^3)	Particle size of mixing sand (mm)	Sand mix proportion (%)
S1	25	1.35	0.15–0.3	0
S2			0.15–0.3	10
S3			0.15–0.3	20
S4			0.15–0.3	30
S5			0.15–0.3	40
S6			0.3–0.6	40
S7			0.6–1.18	40
S8			1.18–2.36	40

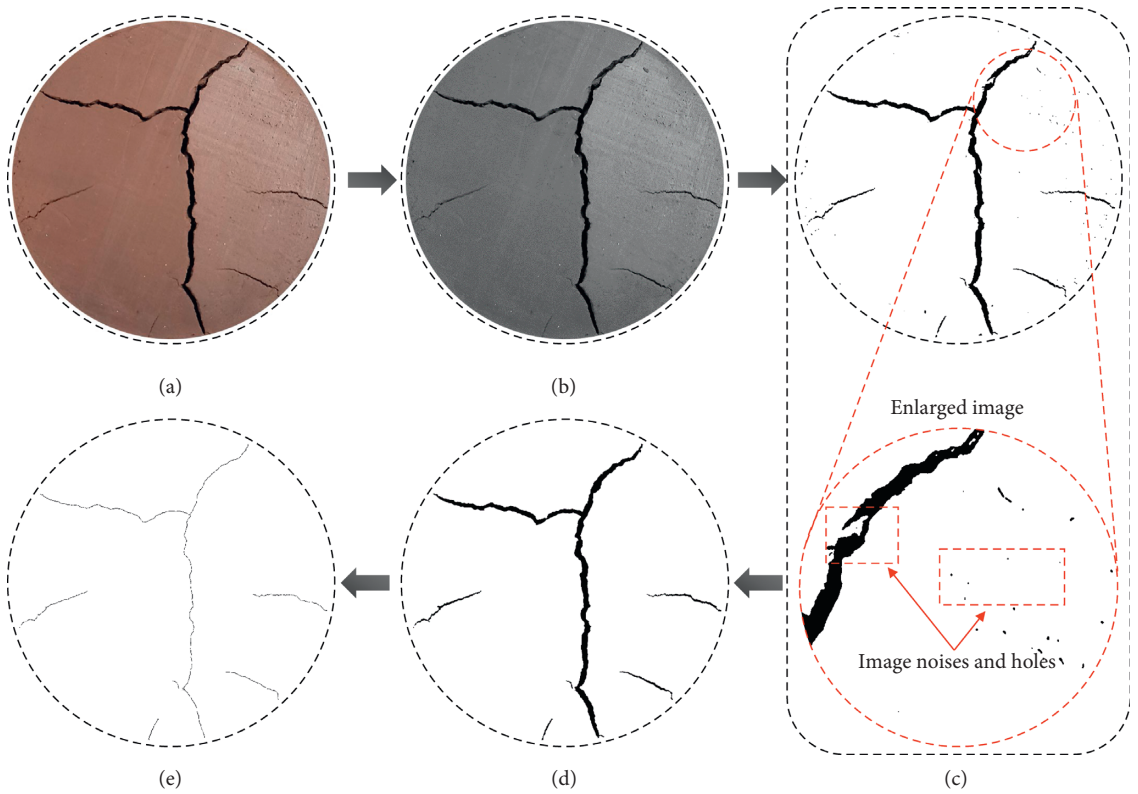

Figure 4: Procedure of digital image processing. (a) Original RGB image, (b) gray level image, (c) binary image, (d) binary image after denoising, and (e) skeleton of the crack network.

longer changed, although the water content in the samples was further reduced. As the sand contents increased from 0 to 40%, the crack ratio reached a stable state at a higher water content, while the final crack ratio decreased sequentially (13.20%, 11.42%, 10.50%, 8.98%, and 7.71%, respectively). Compared with the control sample, the sample with 40% sand content had a 41.7% reduction in surface crack ratio.

Figure 6(b) presents the variation of the crack ratio over the water content under the same sand content (40%) but different particle size groups. As the sand size group increased from 0.15–0.3 mm to 1.18–2.36 mm, the final surface crack ratio showed a downward trend (7.71%, 7.69%, 4.35%, and 3.73%, respectively). Besides, the crack ratio would reach a stable state more quickly as the particle size of the sand increased, reflecting the final state where the cracks no longer developed in the process of evaporation. Figure 6(c) is a representative image of the final cracking state of the samples in S1–S8. It could be observed that, in this experimental design, the surface crack ratio decreased with the increase in sand contents under the same particle size group condition; when the sand content was the same, the crack ratio decreased with the increase in sand particle size.

Take the sample with a sand content of 0 as an example; Figure 7 shows the variation of crack ratio, crack length, and average crack width over water content during the evaporation process. The crack ratio continued to increase when the water content was greater than 9%. The water content of the cracking images I, II, and III inserted in Figure 7 was 23.52%, 22.03%, and 19.5%, respectively. Specifically, the increasing crack ratio was characterized by the increase in the crack length when the water content was greater than 19.5%. The crack length had remained stable and no longer grew when the water content was greater than 9% and less than 19.5%. At this time, the surface tensile stress was fully

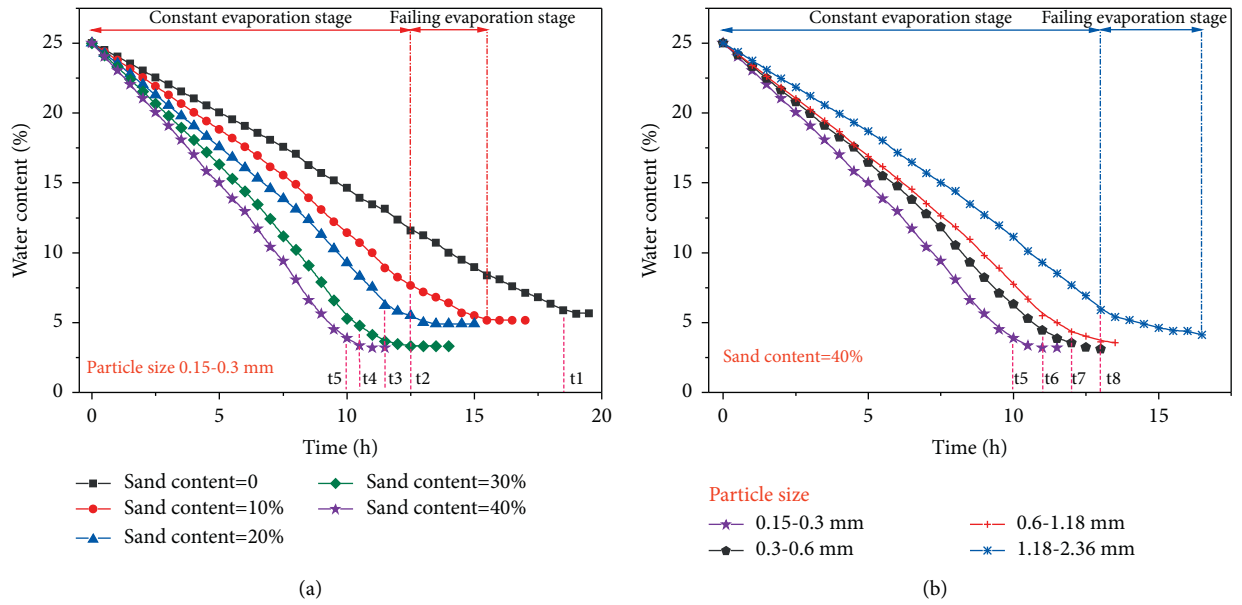

Figure 5: Variation of water content over time of soil samples under the effect of different sand contents and particle sizes. (a, b) Time (h).

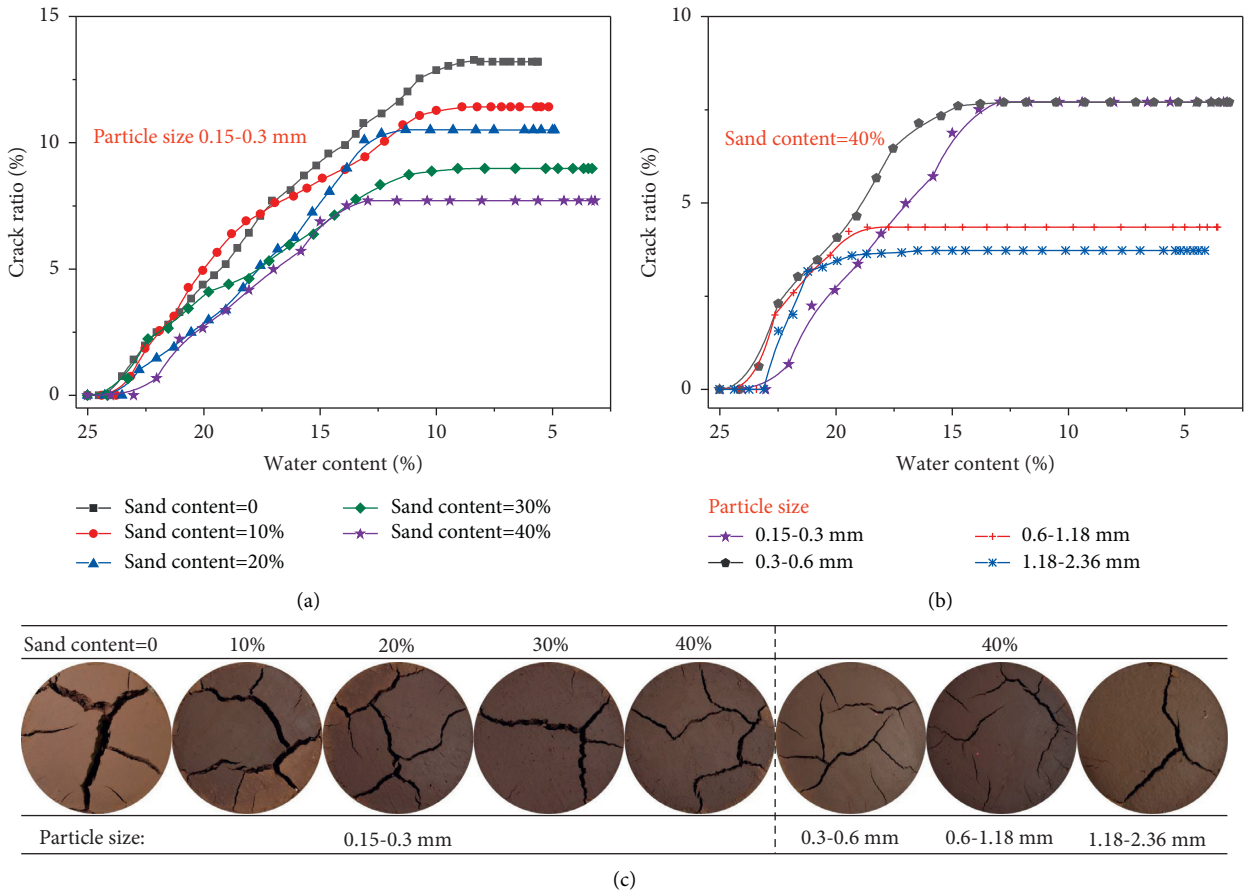

Figure 6: Variation of the crack ratio over water content of soil samples under the effect of different sand contents and particle sizes: (a) the effect of different sand contents on crack ratio; (b) the effect of sands with different particle sizes on crack ratio; (c) the final state of surface cracks.

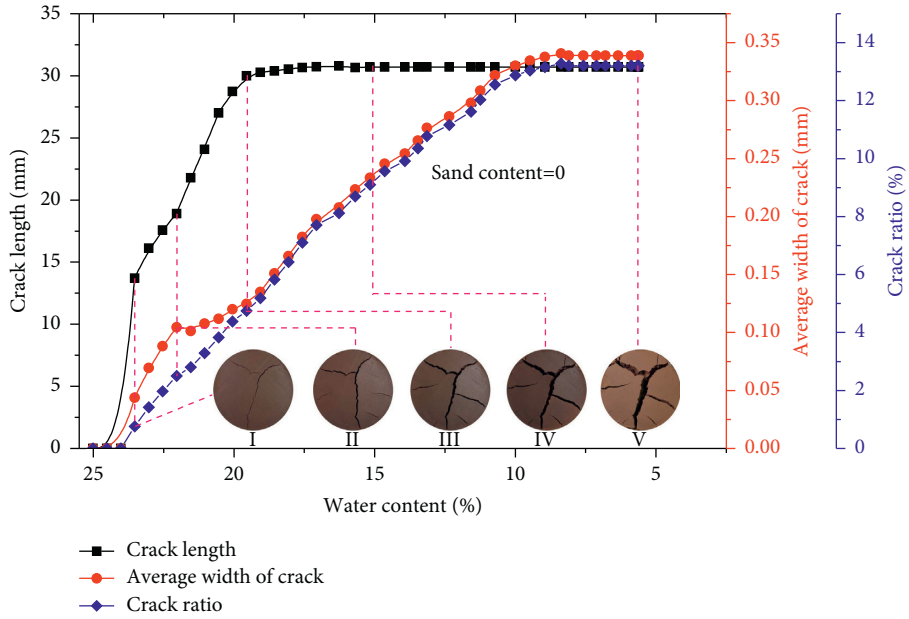

Figure 7: Variation of crack length, the average width of the crack, and crack ratio over water content (sand content = 0).

released, and the tensile strength of the soil gradually increased, leading to a smaller possibility for new cracks in the subsequent drying process. Consequently, the phenomenon of increasing cracking area was manifested in the continuous widening of the cracks. Therefore, the development of desiccation cracks in compacted soil samples was dominated by the increase in crack length in the early stage. Furthermore, the increase in the crack area was controlled by the increase in crack width when the crack network was stabilized.

The fractal dimension can reflect the irregularity of the cracking network. The larger the fractal dimension, the more developed the cracks. Once cracks appeared in the compacted soil sample, the basic morphology of the cracking network was established, as illustrated in Figure 8(a). Therefore, the fractal dimension of the surface crack increased instantaneously after crack initiation, as presented in Figures 8(a) and 8(b). During the drying process, the fractal dimension increased with the development of the cracking network. When the cracking development was stable, the fractal dimension no longer changed. In Figure 8(a), the final cracking fractal dimension decreased from 1.61 to 1.49 as the sand content increased from 0 to 40%. In Figure 8(b), the fractal dimension of the cracks decreased from 1.49 to 1.39 as the sand size increased from [0.15, 0.3) to [1.18, 2.36). This also suggested that the increase of sand content and sand particle size group could inhibit the development of cracks in compacted soil samples.

4. Discussion

Adding a proper amount of sand into expansive soil could reduce the proportion of clay minerals, improve the gradation of expansive soil, and change the physical and mechanical properties of expansive soil, such as the optimal water content, maximum dry density, Atterberg limits, and strength characteristics. Besides, the expansion and shrinkage properties during the dry-wet cycle also change [27, 28].

4.1. Effect of Sand Content and Particle Size on Water Evaporation. The evaporation process of samples with different sand contents and particle size groups could be divided into three stages: constant evaporation, failing evaporation, and residual water content stage. The external factors affecting the evaporation rate mainly include temperature, relative humidity, and wind speed, while the internal factors mainly include the mineral composition, particle size, water content, and degree of compaction of the soil [14, 29]. The initial water content, dry density, and evaporation environment of the samples were the same in the test. The main factor affecting the evaporation rate was the changes in soil properties caused by the sand content and particle size group in soil.

The migration of water inside the soil to the surface is mainly controlled by capillary action. Furthermore, the migration of capillary water is influenced by the pore size between particles in the soil. As the sand content in the expansive soil increased, the macropores formed between sand particles were not enough to be filled by fine-grained soil. As a result, the water holding capacity of the samples decreased, leading to a higher evaporation rate and lower residual water content. Under the same sand content condition, the strength of the soil sample skeleton and the volume shrinkage capacity of the sample increased and decreased, respectively, as the particle size of the sand increased, causing a decrease in the surface desiccation crack areas. Therefore, the evaporation rate was smaller, and the residual water content also exhibited an increasing trend as the particle size groups increased. As the evaporation

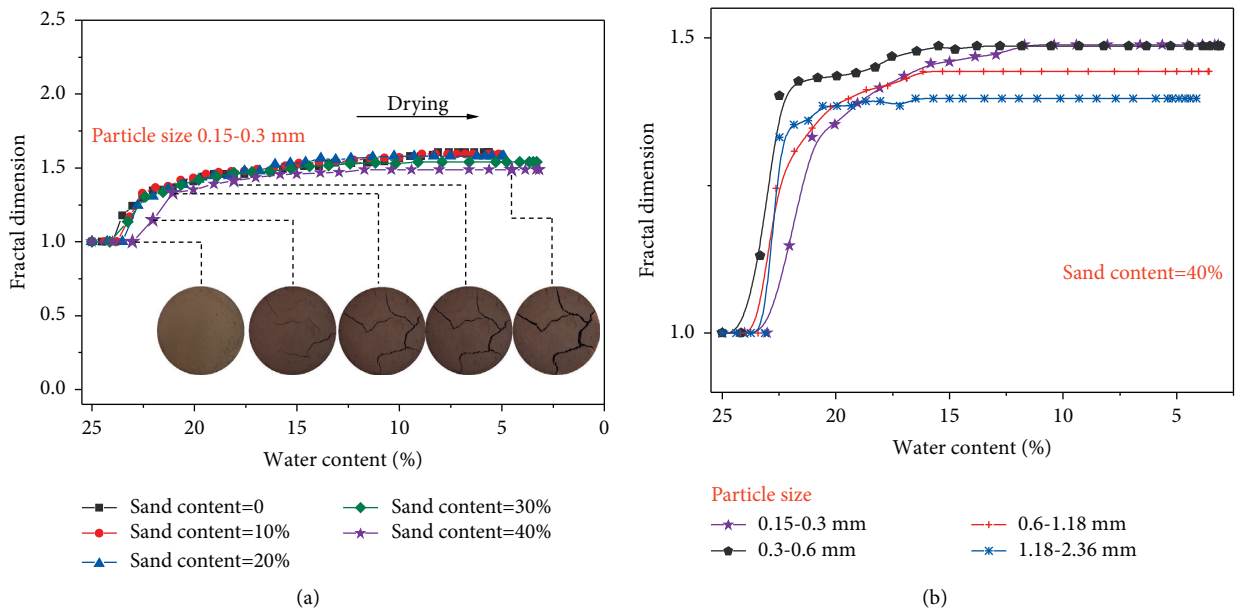

FIGURE 8: Variation of fractal dimension over water content of soil samples under the effect of different sand contents and particle size. (a, b) Water content (%).

continued, the water evaporation mechanism of the soil sample changed from the migration of capillary water to the diffusion of water vapor and then entered the failing evaporation stage. The evaporation stopped and entered the residual water content stage when the vapor pressure inside the sample was in equilibrium with the external environment.

4.2. Effect of Sand Content and Particle Size on Desiccation Cracks. At the beginning of the test, the soil sample surface was the only evaporation channel. Then, the water gradient was generated along the axial direction in the sample. The surface water content of the sample was less than the internal of the sample, while the surface shrinkage was greater than the internal soil under the action of matrix suction. Hence, the tensile stress field formed on the sample surface. Cracks appeared when the tensile stress is greater than the tensile strength [30]. Besides, if the tensile stress is less than the tensile strength, the shrinkage deformation of the compacted soil sample mainly manifests as volume shrinkage until it reaches the shrinkage limit of the soil [31].

After the addition of sand into the expansive soil, the existence of large-size sand effectively improved the friction between particles of the mixture and thus enhanced the skeleton strength of sand-modified expansive soil. As the sand contents increased, macropores in the soil were formed between sand particles, and between sands and soil aggregates. The existence of large pores can reduce the matrix suction in the soil. Therefore, the crack ratio of the soil sample surface decreased as the sand contents increased. When the sand content was the same, the larger the sand particle size, the easier it was to induce the macroporous structure between the particles, just like the effect of the increase of sand content. Meanwhile, the friction between the particles increased, leading to an increasing in the strength of the soil skeleton. Therefore, the surface crack ratio decreased with the increase in the sand particle size groups.

4.3. Effect of Boundary Conditions on Desiccation and Shrinkage. Tensile stress would generate inside the material when the shrinkage of the material is restricted. The magnitude and distribution of tensile stress depend on the stiffness of the material, the boundary conditions, and the stress concentration effect caused by potential defects in the material [13, 32]. In the test, the sample was prepared in a glass container, in which the bonding force between wet soil and glass was large initially and even larger after drying. The bottom and surroundings of the sample were subject to the constraints from the contacts of the glass container. This may be the reason that only desiccation cracks appeared in the above samples with no centripetal shrinkage. The stainless-steel ring knives with the same inner diameter and height of the glass container were customized to investigate the influence of boundary conditions on the shrinkage of the sample. Vaseline was smeared on the inner wall of the ring knife to prepare compacted soil samples with the same initial state as S1–S5 (namely, the initial water content was 25%, the dry density was 1.35 g/cm^3, the particle size of the group was [0.15–0.3 mm), and the sand content was 0–40%). Drying tests were performed under the same conditions. The samples eventually all presented volume shrinkage with no desiccation cracks, as illustrated in Figure 9. The surface shrinkage ratio is defined as the ratio of the reduction of the surface area caused by sample shrinkage to the area of the ring knife. With the increasing sand content from 0 to 40%, the surface shrinkage ratio was 27.38%, 25.88%, 24.14%, 21.06%, and 17.45%, respectively. Thus, the expansive soil

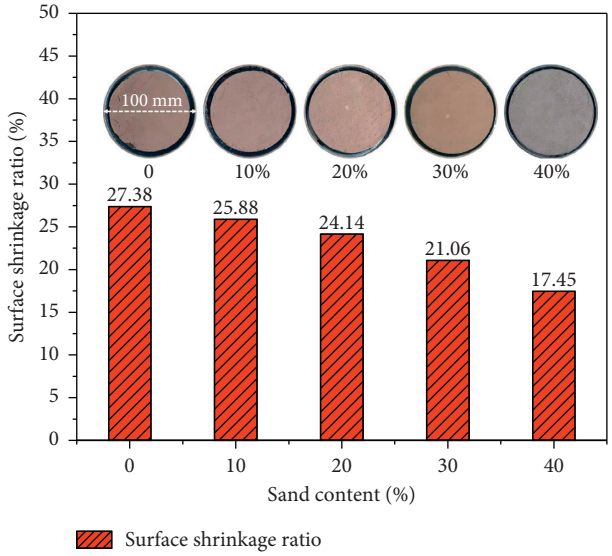

Figure 9: Final surface shrinkage ratio of compacted soil sample in ring knife.

improved by sands effectively reduced the shrinkage phenomenon.

5. Conclusions

In this study, a series of drying tests of compacted soil samples with the same initial dry density and water content were prepared to investigate the influence of sand content and particle size group on the desiccation cracks of compacted expansive soil. The following conclusions were obtained.

The evaporation process of compacted soil could be divided into three stages: constant evaporation, failing evaporation, and residual water content stage. With the increasing sand content and the sand particle group, the evaporation rate and the residual water content increased and decreased, respectively. The surface crack ratio decreased with the increase in the sand content. For the same sand content, it also decreased with the increase in the sand particle size. The variation of fractal dimension was consistent with the crack ratio. The increase of the surface crack ratio in the early stage was manifested as the increase of cracking length, and that in the later stage was characterized by the increase of cracking width. Affected by the boundary conditions, the shrinkage deformation of compacted expensive soil samples could present the phenomenon of centripetal shrinkage or cracking.

The results of this study verify the effectiveness of sand in restraining the shrinkage deformation of expansive soil. However, the strength characteristics, permeability, and deformation characteristics of the sand-improved soil should be further considered in conjunction with specific application conditions to meet the engineering requirements.

Data Availability

The data used to support the findings of this study are available from the corresponding author upon request.

Conflicts of Interest

The authors declare that they have no conflicts of interest.

Acknowledgments

The laboratory portion of this study was carried out in the Soil Mechanics Laboratory of the School of Civil and Architecture Engineering, Xi'an Technological University, in which physical and mechanical parameters of soil were tested and provided by the graduate student Wei Chen. The authors sincerely thank the authority of the School of Civil and Architecture Engineering and the help provided by Prof. He Hui and Prof. Li Baoping. This work was supported by Xi'an Key Laboratory of Civil Engineering Testing and Destruction Analysis on Military-Civil Dual-Use Technology.

References

[1] S. Fityus and O. Buzzi, "The place of expansive clays in the framework of unsaturated soil mechanics," *Applied Clay Science*, vol. 43, no. 2, pp. 150–155, 2009.

[2] A. R. Estabragh, M. R. S. Pereshkafti, B. Parsaei, and A. A. Javadi, "Stabilised expansive soil behaviour during wetting and drying," *International Journal of Pavement Engineering*, vol. 14, no. 4, pp. 418–427, 2013.

[3] S. Qi and S. K. Vanapalli, "Influence of swelling behavior on the stability of an infinite unsaturated expansive soil slope," *Computers and Geotechnics*, vol. 76, pp. 154–169, 2016.

[4] J. Somasundaram, R. Lal, N. K. Sinha et al., "Cracks and potholes in vertisols: characteristics, occurrence, and management," in *Advances in Agronomy*, D. L. Sparks, Ed., vol. 149pp. 93–159, 2018.

[5] Q. Cheng, C.-S. Tang, D. Xu, H. Zeng, and B. Shi, "Water infiltration in a cracked soil considering effect of drying-wetting cycles," *Journal of Hydrology*, vol. 593, Article ID 125640, 2021.

[6] L. Cao, Z. Wang, and Y. Chen, "Unsaturated seepage analysis of cracked soil including development process of cracks," *Advances in Materials Science and Engineering*, vol. 2016, Article ID 2684297, 2016.

[7] S. Utili, "Investigation by limit analysis on the stability of slopes with cracks," *Géotechnique*, vol. 63, no. 2, pp. 140–154, 2013.

[8] L. Zhu, D. Fan, R. Ma, Y. Zhang, and Y. Zha, "Experimental and numerical investigations of influence on overland flow and water infiltration by fracture networks in soil," *Geofluids*, vol. 2018, Article ID 7056858, 2018.

[9] J. Zhang, D. Zhu, and S. Zhang, "Shallow slope stability evolution during rainwater infiltration considering soil cracking state," *Computers and Geotechnics*, vol. 117, Article ID 103285, 2020.

[10] C. Lozada, B. Caicedo, and L. Thorel, "Effects of cracks and desiccation on the bearing capacity of soil deposits," *Géotechnique Letters*, vol. 5, no. 3, pp. 112–117, 2015.

[11] S. Bordoloi, J. Ni, and C. W. W. Ng, "Soil desiccation cracking and its characterization in vegetated soil: a perspective review," *The Science of the Total Environment*, vol. 729, Article ID 138760, 2020.

[12] C.-S. Tang, C. Zhu, Q. Cheng et al., "Desiccation cracking of soils: a review of investigation approaches, underlying mechanisms, and influencing factors," *Earth-Science Reviews*, vol. 216, Article ID 103586, 2021.

[13] S. Costa, J. Kodikara, and B. Shannon, "Salient factors controlling desiccation cracking of clay in laboratory experiments," *Géotechnique*, vol. 63, no. 1, pp. 18–29, 2013.

[14] C. Tang, B. Shi, C. Liu, L. Zhao, and B. Wang, "Influencing factors of geometrical structure of surface shrinkage cracks in clayey soils," *Engineering Geology*, vol. 101, no. 3, pp. 204–217, 2008.

[15] M. Abou Najm, J. Jesiek, R. H. Mohtar, P. Lura, and G. Sant, "Assessing the role of the pore solution concentration on horizontal deformations in an unsaturated soil specimen during drying," *Geoderma*, vol. 187-188, pp. 31–40, 2012.

[16] N. Yesiller, C. J. Miller, G. Inci, and K. Yaldo, "Desiccation and cracking behavior of three compacted landfill liner soils," *Engineering Geology*, vol. 57, no. 1, pp. 105–121, 2000.

[17] C. C. Ikeagwuani and D. C. Nwonu, "Emerging trends in expansive soil stabilisation: a review," *Journal of Rock Mechanics and Geotechnical Engineering*, vol. 11, no. 2, pp. 423–440, 2019.

[18] S. Y. Amakye and S. J. Abbey, "Understanding the performance of expansive subgrade materials treated with non-traditional stabilisers: a review," *Cleaner Engineering and Technology*, vol. 4, Article ID 100159, 2021.

[19] R. M. AlZubaidi, K. H. AlRawi, and A. J. AlFalahi, "Using cement dust to reduce swelling of expansive soil," *Geomechanics and Engineering*, vol. 5, no. 6, pp. 565–574, 2013.

[20] G. Stoltz, O. Cuisinier, and F. Masrouri, "Multi-scale analysis of the swelling and shrinkage of a lime-treated expansive clayey soil," *Applied Clay Science*, vol. 61, pp. 44–51, 2012.

[21] E. Kalkan, "Impact of wetting-drying cycles on swelling behavior of clayey soils modified by silica fume," *Applied Clay Science*, vol. 52, no. 4, pp. 345–352, 2011.

[22] S. B. Ikizler, M. Aytekin, and M. Vekli, "Reductions in swelling pressure of expansive soil stabilized using EPS geofoam and sand," *Geosynthetics International*, vol. 16, no. 3, pp. 216–221, 2009.

[23] D. Li, B. Yang, Z. Gao, and L. Sun, "The effects of biomass ash on soil evaporation and cracking," *Arabian Journal of Geosciences*, vol. 14, no. 10, 2021.

[24] B. Yang, D. Li, S. Yuan, and L. Jin, "Role of biochar from corn straw in influencing crack propagation and evaporation in sodic soils," *Catena*, vol. 204, Article ID 105457, 2021.

[25] K. A. Abera, K. N. Manahiloh, and M. Motalleb Nejad, "The effectiveness of global thresholding techniques in segmenting two-phase porous media," *Construction and Building Materials*, vol. 142, pp. 256–267, 2017.

[26] B. Yang and J. Yuan, "Application of fractal theory to characterize desiccation cracks in contaminated clayey soils," *Arabian Journal of Geosciences*, vol. 12, no. 3, p. 85, 2019.

[27] F. S. Khan, S. Azam, M. E. Raghunandan, and R. Clark, "Compressive strength of compacted clay-sand mixes," *Advances in Materials Science and Engineering*, vol. 2014, Article ID 921815, 2014.

[28] Y. Tan, H. Zhang, and Y. Wang, "Evaporation and shrinkage processes of compacted bentonite-sand mixtures," *Soils and Foundations*, vol. 60, no. 2, pp. 505–519, 2020.

[29] W.-K. Song, Y.-J. Cui, A. M. Tang, W.-Q. Ding, and Q. Wang, "Experimental study on water evaporation from compacted clay using environmental chamber," *Canadian Geotechnical Journal*, vol. 53, no. 8, pp. 1293–1304, 2016.

[30] T. Hueckel, B. Mielniczuk, M. S. El Youssoufi, L. B. Hu, and L. Laloui, "A three-scale cracking criterion for drying soils," *Acta Geophysica*, vol. 62, no. 5, pp. 1049–1059, 2014.

[31] Y. Wang, Y.-J. Cui, A. M. Tang, N. Benahmed, M. Duc, and W. J. Sun, "Shrinkage behaviour of a compacted lime-treated clay," *Géotechnique Letters*, vol. 10, no. 2, pp. 174–178, 2020.

[32] H. Peron, T. Hueckel, L. Laloui, and L. B. Hu, "Fundamentals of desiccation cracking of fine-grained soils: experimental characterisation and mechanisms identification," *Canadian Geotechnical Journal*, vol. 46, no. 10, pp. 1177–1201, 2009.